Bulletin of the Seismological Society of America, Vol. 103, No. 4, pp. 2188–2202, August 2013, doi: 10.1785/0120120132

Multiscale Mapping of Completeness Magnitude of Earthquake Catalogs

by I. Vorobieva,* C. Narteau, P. Shebalin,* F. Beauducel, A. Nercessian, V. Clouard,* and M.-P. Bouin*

Abstract We propose a multiscale method to map the spatial variations of the completeness magnitude M_c of earthquake catalogs. The Gutenberg–Richter law describing the earthquake frequency–magnitude distribution (FMD) might not hold over the entire magnitude range, and small areas may exhibit a specific type of seismicity, especially in volcanotectonic contexts. For these reasons, any scaling relation should be obtained by adapting the dimension of the studied zone to the range of the event magnitude. Here, we associate ranges of larger magnitudes with increasing areas for data selection based on empirical relations in seismotectonics. Then, for each point in space, we document the earthquake FMD at all length scales within the corresponding earthquake magnitude ranges. High resolution of the M_c-value is achieved through the determination of the smallest space–magnitude scale in which the Gutenberg–Richter law is verified. The multiscale procedure isolates the magnitude range that meets the best local seismicity and local record capacity. Using artificial catalogs and earthquake catalogs of the Lesser Antilles arc, this M_c-mapping method is shown to be efficient in regions with mixed types of seismicity, a variable density of epicenters, and various levels of registration.

Introduction

Earthquake catalogs are an important product of observational seismology, and they are used as input data for numerous studies in earthquake physics, tectonics, and seismic-hazard analysis. Because catalogs always have a lower limit for recording, each of them has to be characterized by a magnitude of completeness M_c and by its variation in space. This problem has been intensively studied over the last two decades, during which many techniques have been developed (see Mignan and Woessner, 2012, for a review). Basically, the minimum magnitude of complete recording may be obtained using network or catalog analysis methods.

Network analysis methods are based on the evaluation of the detection capability of a given distribution of seismic stations (Gomberg, 1991; Kvaerna *et al.*, 2002a,b; Nanjo, Schorlemmer, *et al.*, 2010). The main advantage of this approach is that the determination of M_c is independent of natural variation of seismic activity. Thus, for example, it can be used to estimate M_c in tectonically stable and aseismic territories. Nevertheless, the quality of the catalog may differ from the theoretical instrumental level of detectability because of technical and administrative factors during data processing. In this case, the solution proposed by Schorlemmer and Woessner (2008) is to implicitly include these factors in the probability distributions of event detection.

Catalog analysis methods are based only on the estimation of the quality of the recorded data (Rydelek and Sacks, 1989; Wiemer and Wyss, 2000; Woessner and Wiemer, 2005). The main advantage of this approach is to rely only on the observations without resorting to material consideration. However, all of these methods are built from *a priori* knowledge about the studied seismicity.

Among all of the empirical power-law statistics of earthquake and fault patterns, the most common is the frequency–size distribution of the earthquake moment (Ishimoto and Iida, 1939; Gutenberg and Richter, 1944). Using the magnitude of an earthquake instead of the moment, in almost all cases the frequency–magnitude distribution (FMD) follows the well-known Gutenberg–Richter (GR) law,

$$\log_{10}(N) = a - bM, \tag{1}$$

so that N is the number of earthquakes within a magnitude range $[M, M + \delta M]$ and the constants a and b are positive. In addition, each of these magnitude ranges may be related to a rupture area R_a using other empirical scaling relations of the form

$$\log_{10}(R_a) = c + dM, \tag{2}$$

in which c and $d > 0$ are two constants (Kanamori and Anderson, 1975; Wells and Coppersmith, 1994). Together,

*Also at Institut de Physique du Globe de Paris, Sorbonne Paris Cité, Univ. Paris Diderot, UMR 7154 CNRS, 1 rue Jussieu, 75238 Paris, Cedex 05, France.

equations (1) and (2) suggest that larger earthquake statistics should be investigated in larger space (Wesnousky, 1994; Molchan *et al.*, 1997).

In a vast majority of cases, catalog-based methods determine the M_c-value by estimating the limit below which the cumulative FMD deviates from the GR law observed for larger magnitude events. For example, this approach includes the maximum-curvature method, the goodness-of-fit test (Wiemer and Wyss, 2000), the M_c- and b-value stability (Cao and Gao, 2002), the entire-magnitude-range method (Ogata and Katsura, 1993; Woessner and Wiemer, 2005), and the median-based analysis of the segment slope (Amorèse, 2007).

However, earthquakes do not always follow universal power-law statistics in all space–time domains (Schorlemmer *et al.*, 2005; Narteau *et al.*, 2009), and these methods may be difficult to implement in regions where various types of seismic regimes coexist (i.e., where the slope b of the FMD is not constant across the entire range of the magnitude). Furthermore, options for spatial data selection may have an impact on M_c-value estimates. Actually, two techniques are commonly used. The first technique is to scan the entire territory with circles of constant radius. For example, this constant area approach is efficient for determining the M_c-value worldwide for the Global (formerly Harvard) Centroid Moment Tensor and the International Seismological Centre ($M > 4$) catalogs using circles with radii of 1000 and 900 km, respectively (Woessner and Wiemer, 2005). Unfortunately, it cannot be used with high spatial resolution given the natural dispersion of the epicenter location. The second technique is to use a constant number of events at each point in space. This constant-sample-size approach was applied successfully for M_c mapping in California, Australia, and Japan (Wiemer and Wyss, 2000; Sagar and Leonard, 2007; Nanjo, Ishibe, *et al.*, 2010). If this method outperforms the constant area approach in terms of resolution, the M_c-value may be biased by sharp changes of seismic activity and/or discontinuous levels of registration (Rydelek and Sacks, 2003). Thus, the sampling problem is a basic shortcoming of catalog-based methods.

Recently, Mignan *et al.* (2011) proposed a comprehensive method for M_c mapping based on the simultaneous analysis of the seismic network configuration and recorded seismicity. This method is decomposed into two steps. First, an iterative procedure estimates both the local radius of the circle for data selection and the M_c-value with respect to the seismic station distribution. In the second step, these locally optimized radii allow the M_c-value to be mapped using classical catalog-based approaches. Then, Bayes theorem is used to combine maps obtained from the iterative procedure and maps predicted from prior knowledge of the proximity of a given location to the seismic stations. This approach is well adapted to a seismic zone with a homogeneous density of seismic stations and a fixed network configuration.

In this paper, we present a new catalog-based approach for M_c mapping in zones with different types of seismicity. The originality of this approach is to analyze earthquake scaling relations across the entire range of length scales documented by the catalog. Because the FMD cannot cover the full range of magnitude in smaller space–time domains, the multiscale procedure is built around a relation between an area for data selection and the range of magnitude over which the GR law has to be investigated.

A Multiscale Method to Map Spatial Variations in M_c

Power-law statistics are ubiquitous in earthquake physics, leading to the idea that the same phenomena may be observed in all space–time domains. Nevertheless, multiple sources of data show the opposite (Ben-Zion, 2008):

1. Seismicity is usually a mixture of different types of events, especially in a volcanotectonic context (Farrell *et al.*, 2009; Segall, 2010). Then, the GR law might not hold over the entire magnitude range due to a superposition of GR laws in specific magnitude ranges.
2. Earthquake ruptures propagate along nonplanar fractures and rupture initiation, propagation, and arrest may be controlled by geometrical and heterogeneous faulting properties (King, 1983; Schwartz and Coppersmith, 1984; Wesnousky, 1994). Then, small regions may be less prone to large events even if there were an infinite number of events in the catalogs.
3. Power laws may have some limits over low and/or high value ranges (Narteau *et al.*, 2002). Furthermore, when these power-law regimes are clearly established, their exponents may have several dependencies; for example, on stress (Narteau *et al.*, 2003, 2009; Schorlemmer *et al.*, 2005).

These observations support the idea that earthquake patterns strongly depend on both the location and size of seismic zones. Hence, it seems clear that scaling relations should only be obtained for earthquakes that are small when compared to the linear size of the considered region (Molchan *et al.*, 1997). Here, we develop this concept for the analysis of the FMD and, more specifically, for the determination of M_c. Basically, we consider a relation between the magnitude range and the characteristic length scale of the domain for data selection. Exploring all ranges of magnitude, we finally get a multiscale description of an entire seismogenic zone. To estimate the M_c-value, we look for the smallest magnitude range for which the GR law is satisfied (Fig. 1).

Multiscale Scanning of the Territory

The earthquake magnitude scale is decomposed into a set of ranges $\mathcal{M}_i = [M_i, M_i + W_M]$ using an overlapping sliding window of constant width W_M and step Δm. The lower limit of the smallest magnitude range is a value given by the smallest earthquake in the catalog. Each earthquake magnitude range $\mathcal{M}_i$ is associated with a circle $\mathcal{C}_i$ of radius

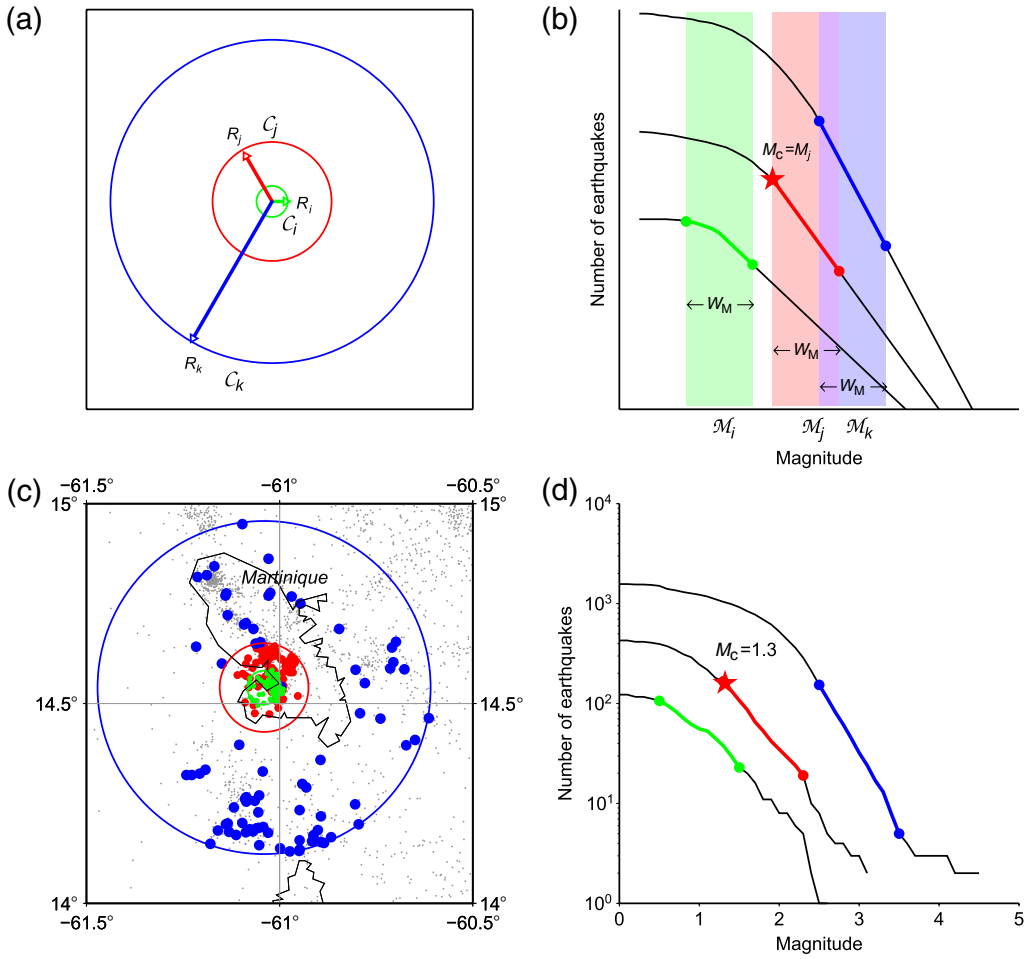

Figure 1. Multiscale mapping of completeness magnitude M_c. At a given point in space, the entire procedure is based on a relation between the area for data selection and the magnitude range over which the corresponding FMD is analyzed. (a) Concentric circles C_i, C_j, and C_k with larger radii R_i, R_j, and R_k are associated with three magnitude ranges $\mathcal{M}_i$, $\mathcal{M}_j$, and $\mathcal{M}_k$ of constant width W_M (shaded areas in [b]). (b) Black lines are the FMDs obtained by selecting all earthquakes in C_i, C_j, and C_k. These FMDs are highlighted within the magnitude range over which we test the consistency of the GR law. As shown by a star in (b), the M_c-value is the lower limit of the smallest magnitude range for which the GR law is satisfied. Parts (c) and (d) show an example in Martinique (14.54° N, 61.04° W) using the OVSG–OVSM catalog from 1996 to 2010. Earthquakes that contribute to the highlighted segments in (d) are shown with the same shadings in (c). The color version of this figure is available only in the electronic edition.

R_i for data selection. Hence, we need to determine a length scale for which the number of events in a given magnitude range is large enough to ensure reliable estimation of the FMD. This length scale may be determined from the distribution of seismic stations as in Mignan *et al.* (2011). Instead, in a catalog-based approach, it is possible to use empirical laws of statistical seismology. For example, assuming a homogeneous density of events and seismic sources, both equations (1) and (2) suggest an exponential relationship of the form

$$R_i = R_0 \times 10^{pM_i}, \tag{3}$$

for which p and R_0 are two positive constants. Dimensional analysis shows that the exponent p should be close to $b/2$ and $d/2$ from equations (1) and (2), respectively. On the other hand, the characteristic length R_0 may be set according to the required number of events or seismic sources within each magnitude range. In practice, given the observed variability of the parameters of equations (1) and (2) in different geophysical settings, we recommend taking a p-value slightly greater than 0.5 and an R_0-value on the order of 1 km. For a vast majority of active seismic zones, these values ensure that the circle's radius R_i is about two orders of magnitude larger than the linear size of earthquake sources of the corresponding magnitude range $\mathcal{M}_i$.

Finally, given the set of magnitude ranges $\mathcal{M}_i$, we end up with a set of circles $\mathcal{C}_i$ that are used for data selection. Thus, we obtain FMDs at different length scales and at every point in space. The originality of the approach is to analyze each FMD within the range of magnitude $\mathcal{M}_i$ that have been used to determine the radius R_i of the circle $\mathcal{C}_i$ (Fig. 1b,d).

Determination of the M_c-Value

Analyzing all the magnitude–space domains $\{\mathcal{M}_i, \mathcal{C}_i\}$ at a given point in space, the M_c-value corresponds to the lower

limit of the smallest range $\mathcal{M}_i$ in which the FMD satisfies the GR law. In practice, we start with the smallest space–magnitude domain and successively test if M_i is M_c according to the following conditions:

- *Condition 1:* The number of events within $\mathcal{C}_i$ in the magnitude range $\mathcal{M}_i = [M_i, M_i + W_M]$ is larger than a constant number N_c.
- *Condition 2:* The FMD within the magnitude range $\mathcal{M}_i = [M_i, M_i + W_M]$ satisfies the GR law (Fig. 1).

A local M_c-value is given by the smallest M_i-value for which these two conditions are met. M_c-value maps are obtained by repeating the procedure at every point in space.

Evaluation of the Consistency of the GR Law for a Given Magnitude Range

Considering that the FMD follows the GR law (equation 1), the b-value may be obtained with the maximum-likelihood point-estimator method. For a continuous (i.e., exact) magnitude distribution and an infinite maximum magnitude, Aki (1965) shows that

$$b = \frac{\log_{10}(e)}{\langle M \rangle - M'}, \tag{4}$$

for which $\langle M \rangle$ is the mean magnitude of $M \geq M'$, and M' is a magnitude for which the catalog is complete. Nevertheless, for a finite maximum magnitude and/or grouped magnitude data, equation (4) gives a biased estimation of the b-value due to biased values of $\langle M \rangle$ and M'. To overcome these issues, Bender (1983) proposes a new set of maximum-likelihood formulas. Based on these formulas, here we develop an iterative procedure to compute the b-value on a given magnitude range $[M_{min}, M_{max}]$.

By definition, we consider that

$$W_M = M_{max} - M_{min} = K\Delta m. \tag{5}$$

Then, we decompose the finite magnitude range $[M_{min} - \Delta m/2,\ M_{max} + \Delta m/2[$ into $K + 1$ bins of constant width Δm. The central value of the kth magnitude bin is

$$M_k = M_{min} + k\Delta m, \tag{6}$$

with $k = \{0, 1, 2, \ldots, K\}$, so that $M_0 = M_{min}$ and $M_K = M_{max}$.

For each bin, n_k and $\langle m \rangle_k$ are the number and the mean magnitude of $M \in [M_k - \Delta m/2, M_k + \Delta m/2[$ earthquakes, respectively. Similarly, N_k and $\langle M \rangle_k$ are the number and the mean magnitude of $M \in [M_k - \Delta m/2, \infty[$ earthquakes, respectively. At the beginning of the iterative procedure, the initial b-value for the entire magnitude range is

$$b_0 = \frac{\log_{10}(N_1) - \log_{10}(N_K)}{M_K - M_1}. \tag{7}$$

For a given b_j-value, an iteration consists of the following steps:

- *Step 1:* Estimation of $\langle M \rangle_K$ taking $M' = M_{max} - \Delta m/2$ and $b = b_j$ in equation (4).
- *Step 2:* Estimation of $\langle m \rangle_k$ and $\langle M \rangle_k$ from $k = K - 1$ to $k = 1$ using successively for each bin k two recursive formulas,

$$\langle m \rangle_k = \frac{\int_{M_k - \Delta m/2}^{M_k + \Delta m/2} \mu 10^{a - b_j \mu} d\mu}{\int_{M_k - \Delta m/2}^{M_k + \Delta m/2} 10^{a - b_j \mu} d\mu} = M_k + \frac{\log_{10}(e)}{b_j} - \frac{\Delta m}{10^{b_j \Delta m} - 1} - \frac{\Delta m}{2} \tag{8}$$

and

$$\langle M \rangle_k = \frac{\langle M \rangle_{k+1} N_{k+1} \langle m \rangle_k n_k}{N_k}. \tag{9}$$

- *Step 3:* Estimation of b_{j+1} taking $\langle M \rangle = \langle M \rangle_1$ and $M' = M_1 - \Delta m/2$ in equation (4).

The iterative process stops when $|b_j - b_{j-1}| < \varepsilon$. In a vast majority of cases, it takes less than 20 iterations to converge to the stationary b-value using $\varepsilon = 10^{-3}$. Nevertheless, if the iterative procedure does not converge after 100 iterations, we consider that the FMD does not follow a GR law within this finite magnitude range $[M_1, M_K]$; that is, $[M_{min} + \Delta m,\ M_{max}]$.

When the iterative procedure converges toward a stationary b-value, we perform an additional test to verify that this slope remains the same throughout the smallest magnitude bin, $M \in [M_0 - \Delta m/2, M_0 + \Delta m/2[$. In fact, we check that there is not a curvature resulting from an incomplete recording of the smallest events. According to Shi and Bolt (1982), we compute the uncertainty δ of our estimation of the b-value:

$$\delta = \frac{b^2}{\log_{10}(e)} \sqrt{\frac{\sum_{k=1}^{K} n_k (M_k - \langle M \rangle_1)^2}{N_1 (N_1 - 1)}}. \tag{10}$$

Then, we check that

$$N_0 \geq N_1 10^{(b-\delta)\Delta m}. \tag{11}$$

If this final condition is met, it is concluded that the GR law with parameter b is satisfied for $M \in [M_{min},\ M_{max}]$ events.

Testing the Multiscale Method on Synthetic Seismic Patterns

To analyze the consistency of the multiscale method and compare it with other methods, we use synthetic catalogs of seismicity to map the M_c-value and estimate the corresponding b-value.

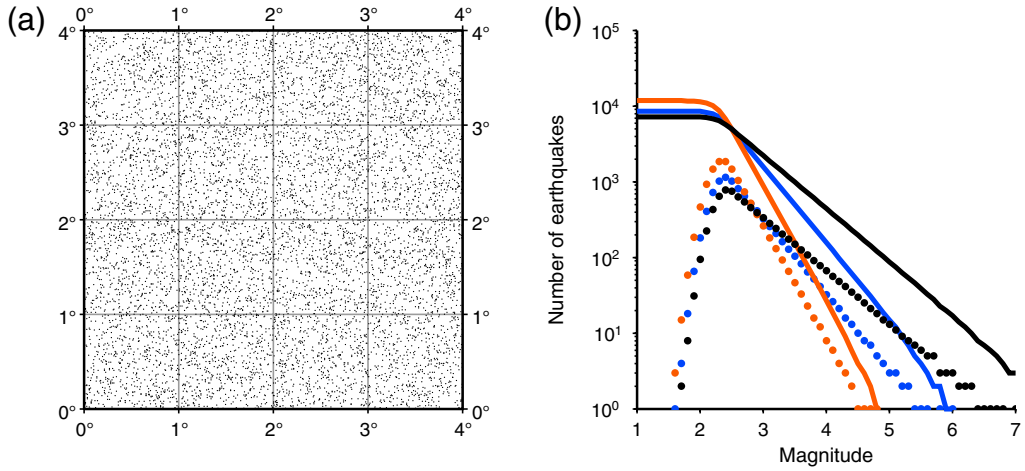

Figure 2. Evaluation of the multiscale method using homogeneous synthetic catalogs. (a) The random distribution of the epicenters. (b) Cumulative (dots) and noncumulative (lines) synthetic FMD distribution for $b = 0.7$, $b = 1.0$, and $b = 1.5$. In all cases, $M_c = 2.5$. The color version of this figure is available only in the electronic edition.

We use grouped magnitude data with an accuracy of 0.1. The territory under investigation is systematically decomposed into grids with square cells of side length 0.02°. At each node of these grids, local FMDs are extracted from the catalogs and then analyzed using $W_M = 1$ and $\Delta m = 0.1$. In addition, we always use a bootstrap technique to calculate the uncertainties δM_c and δb of our local estimates of the M_c and b-values. In practice, we randomly select from the original set of data the same number of events using a sampling scheme with replacement. From 100 of these bootstrap samples, δM_c and δb are defined as the standard deviation of the corresponding sets of M_c and b-values.

Tests on Homogeneous Seismic Patterns

Synthetic catalogs contains $N_0 = 5000$ events of magnitude larger than M_c randomly and homogeneously distributed within a square of side length 4° (Fig. 2a). In all these catalogs, FMDs follow a GR law of slope parameter b above the M_c-value (Fig. 2b). Below, we use a normal distribution as the detection function to reproduce catalog incompleteness. Then, considering a discrete set of magnitude values,

$$M_i = M_c + i\Delta m \quad \text{with} \quad i \in \mathbb{Z}, \tag{12}$$

we have

$$n(M_i) = \begin{cases} N_0(1 - 10^{-b\Delta m})10^{-b(M_i - M_c)} & \text{for } i = 0, 1, 2, \ldots, \\ N_0(1 - 10^{-b\Delta m})10^{-b(M_i - M_c)} \times 10^{-3(M_i - M_c)^2} & \text{for } i = -1, -2, -3, \ldots, \end{cases} \tag{13}$$

for which $n(M_i)$ is rounded to the nearest integer. Using these earthquake patterns with $M_c = 2.5$, we analyze the output of the multiscale procedure for different b-values. Simultaneously, we also vary R_0 and p-values to evaluate the influence of the magnitude–space domains (see equation 3). All the results are presented in Table 1 using the mean and the standard deviation of the distributions of M_c and b-values obtained across the entire territory. These results show that the output of the multiscale method are always in good agreement with the input values. Most importantly, these estimates are not affected by changes in b-values. Similarly, the effect of the p-value is negligible for the particular range of values explored here. Nevertheless, Table 1 also shows that the standard deviations of M_c and b-values decrease with an increasing R_0-value as the result of an increasing number of selected events.

Tests on Heterogeneous Seismic Patterns

To evaluate how the multiscale method is able to distinguish territories with different levels of seismicity and detection capability, we generate artificial catalogs in which zones of high detectability ($M_c = 1$) are surrounded by zones of low detectability ($M_c = 2.5$). We combine these changes in detectability with different levels of seismic activity (Fig. 3a). In the northern area, the level of seismic activity of the zone of low detectability is five times the level of seismic activity of the zone of high detectability. This is opposite in the southern area. For each of these zones, synthetic FMDs are given by equation (13) with $b = 1$ but different N_0-values (Fig. 3b).

Figure 3c shows that the M_c map obtained with the multiscale method is in agreement with the input data. The multiscale method demonstrates high resolution capacity and

Table 1
Parametric Study of the Multiscale Approach Using Homogeneous Synthetic Catalogs

		$b = 0.7$				$b = 1.0$				$b = 1.5$			
p	R_0(km)	$\langle M_c \rangle$	σ_{M_c}	$\langle b \rangle$	σ_b	$\langle M_c \rangle$	σ_{M_c}	$\langle b \rangle$	σ_b	$\langle M_c \rangle$	σ_{M_c}	$\langle b \rangle$	σ_b
0.4	1.2	2.53	0.070	0.70	0.059	2.49	0.069	1.01	0.087	2.47	0.065	1.51	0.134
	2.0	2.51	0.065	0.70	0.037	2.51	0.062	1.00	0.058	2.53	0.078	1.52	0.097
	2.8	2.52	0.056	0.70	0.027	2.53	0.056	1.00	0.042	2.54	0.076	1.52	0.075
	4.0	2.52	0.049	0.69	0.018	2.52	0.040	1.00	0.022	2.53	0.057	1.51	0.045
0.5	1.2	2.54	0.094	0.70	0.064	2.52	0.072	1.01	0.092	2.46	0.061	1.50	0.142
	2.0	2.51	0.070	0.70	0.043	2.51	0.063	1.00	0.063	2.52	0.077	1.52	0.102
	2.8	2.52	0.059	0.70	0.030	2.52	0.058	1.00	0.047	2.54	0.078	1.51	0.081
	4.0	2.53	0.051	0.69	0.020	2.53	0.046	1.00	0.026	2.53	0.063	1.51	0.051
0.6	1.2	2.54	0.075	0.70	0.068	2.55	0.102	1.02	0.089	2.44	0.060	1.48	0.149
	2.0	2.51	0.080	0.70	0.047	2.50	0.086	1.00	0.076	2.51	0.077	1.51	0.109
	2.8	2.51	0.062	0.69	0.033	2.52	0.059	1.00	0.051	2.53	0.079	1.51	0.088
	4.0	2.52	0.053	0.69	0.022	2.51	0.049	1.00	0.032	2.52	0.068	1.50	0.058

Events are randomly distributed in space with $M_c = 2.5$ (see Fig. 2). $\langle M_c \rangle$ and σ_{M_c} are the mean and standard deviation of the M_c-values obtained accross the entire territory. $\langle b \rangle$ and σ_b are the mean and standard deviation of the b-values obtained across the entire territory.

efficiency even with sharp contrasts in seismic activity and level of detection. Nevertheless, when both properties change simultaneously, the M_c-value of more seismically active zones expands slightly into zones of lower activity (see transitions from inner to outer squares in Fig. 3c). This experiment on synthetic catalogs also shows that variations of seismic activity under the condition of equal detectability does not influence the determination of the M_c-value (i.e., from the northern to the southern area in Fig. 3c).

The δM_c map shows that uncertainties remain small in regions with a homogeneous level of seismicity and a constant M_c-value. However, a high δM_c-value may correspond to sharp changes in the detection capability (i.e., from inner to outer squares in Fig. 3c). In fact, the bootstrap procedure detects these discontinuities because the same family of events may be selected by a variety of combinations to the detriment of the other. Note that such a property may help to identify abrupt changes in the M_c of earthquake catalogs.

Most importantly, Figure 3c–h shows how the multiscale method combines the advantages of classical catalog-based methods. An important difference with the constant radius method is that space–magnitude domains simultaneously explore a wide range of circle radii. Thus, the multiscale method takes advantage of the high resolution given by the small circles (see Fig. 3d–f) without the limitations associated with a small number of events in zones of low seismic activity (e.g., blank zones in Fig. 3e,f).

The resolution of the multiscale method is also better than for the constant sample method (Fig. 3g,h). In fact, space–magnitude domains ensure that there is one-to-one correspondence between the M_c-value and the size of the circle for data selection. It guarantees that small and distant earthquakes do not influence the local estimation of the M_c-value. Indeed, we take smaller events out of consideration as we increase the area for data selection. This is not the case for the constant sample method, which therefore may be biased by nonlocal seismic patterns (see the southern area of Fig. 3g,h).

The multiscale method also ensures a minimum number of events within the magnitude range in which we identify the M_c-value. When compared to the constant sample method, there is a gain in precision even for the same minimum sample size (compare the δM_c maps of Fig. 3c and 3h).

Testing Bimodal FMD

Synthetic bimodal FMDs are generated using the heterogeneous seismicity of Figure 3a at the position 0.7° N and 0.7° E in a zone of moderate recording capacity. Figure 4a shows the family of cumulative FMDs obtained from concentric circles for data selection. For the smaller radii (i.e., a smaller number of events), the distributions do not follow the GR law, especially in the corresponding magnitude ranges (highlighted segments). For the larger radii (i.e., a larger number of events), a bimodal shape appears over the entire magnitude range as the circles include the zone with a better detection level. Nevertheless, a single GR law may be observed in the ranges of larger magnitudes associated with larger radii for data selection. Thus, for the smallest magnitude range at which the GR law is respected, the multiscale method is able to capture the local M_c-value of 2.5 (the star in Fig. 4a).

Using a constant radius method with $R = 35$ km at the same location, the M_c-value is significantly underestimated because of the influence of the increasing number of events recorded at larger distances (the triangle in Fig. 4a). Similarly, the constant sample method with 250 events yields a smaller M_c-value because of the influence of nonlocal events (the square in Fig. 4a).

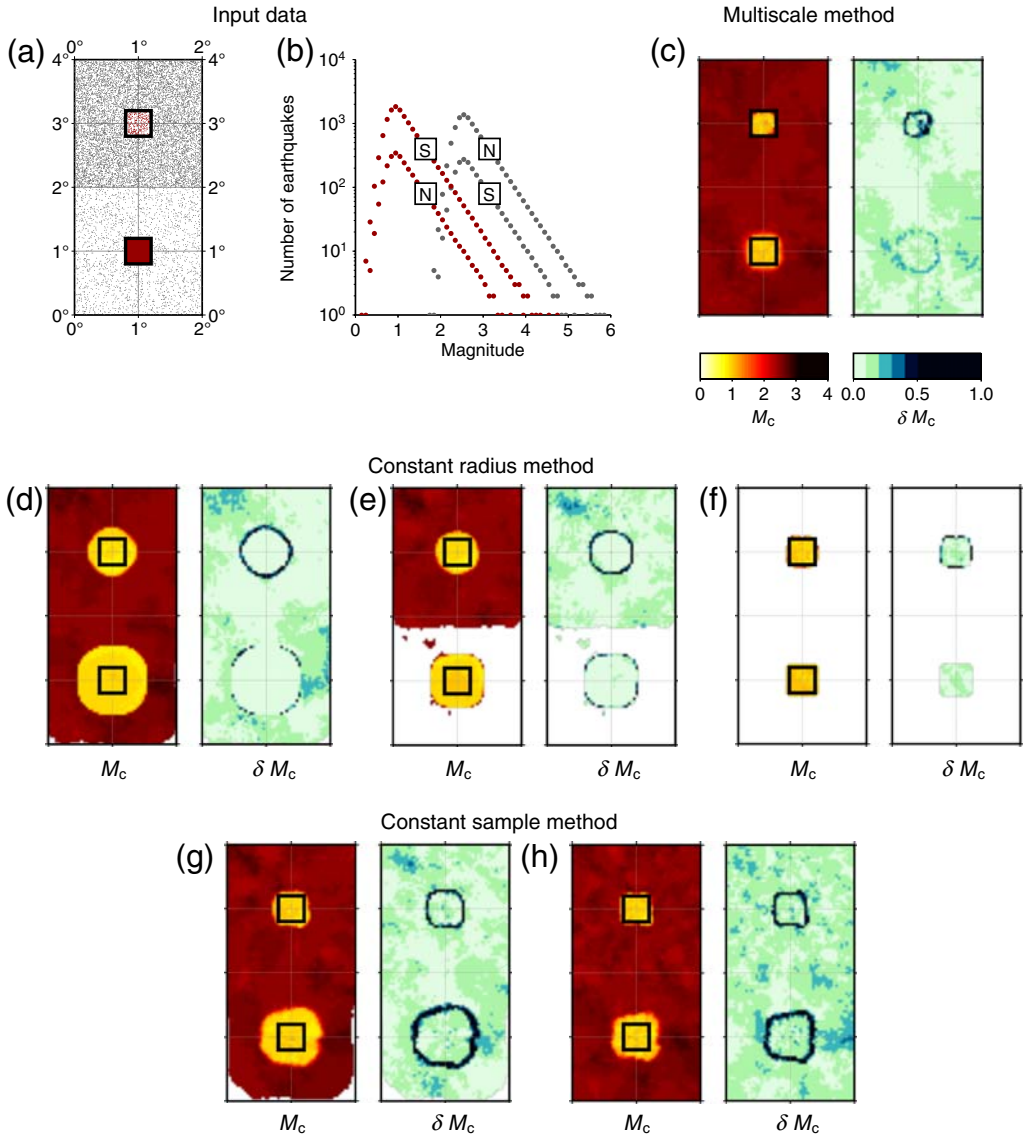

Figure 3. Evaluation of the multiscale method using synthetic catalogs with heterogeneous M_c-value and event density. (a) Distribution of epicenters. (b) Noncumulative FMDs in the northern (N) and the southern (S) areas. In regions of high (north) and low (south) seismic activity, we consider a central area with a better level of completeness ($M_c = 1.0$) than in the surrounding regions ($M_c = 2.5$). (c) M_c-value (left) and δM_c-value (right) maps obtained with the multiscale method ($R_0 = 1.3$ km, $p = 0.6$, $W_M = 1$, $\Delta m = 0.1$, $N_c = 100$) and a bootstrap technique (see text). Similar maps obtained by the most popular methods are shown for comparison using the constant radius method with a radius of (d) 35 km, (e) 22 km, and (f) 8 km and the constant sample size method with (g) 250 events and (h) 100 events. Zones for which it is impossible to evaluate the M_c-value are blank. The color version of this figure is available only in the electronic edition.

Finally, we also test the entire magnitude range (EMR) method proposed by Woessner and Wiemer (2005). Figure 4b shows the noncumulative FMD obtained with a radius of 35 km at the same position as in Figure 4a (see the upper thick line in Fig. 4a), as well as the best solution and the M_c-value predicted by the EMR method. As the estimation of the parameter values is based on a maximum likelihood method, the numerical procedure that evaluates the magnitude threshold between a GR law (for larger magnitudes) and a parabolic decay (for smaller magnitudes) may choose a mode (black arrow in Fig. 4a) that does not correspond to the local M_c (white arrow in Fig. 4a). In this case, the multiscale method may provide an additional layer of information by separating and identifying the different seismic regimes.

Testing the Multiscale Method in the Lesser Antilles Volcanic Island Arc

Volcanic island arcs exhibit specific types of seismic patterns and impose strong constraints on the geometry of the local seismic network. For this reason, the evaluation of spatial variations of the M_c is still a challenge in these zones where all methods may not perform equally well. In our

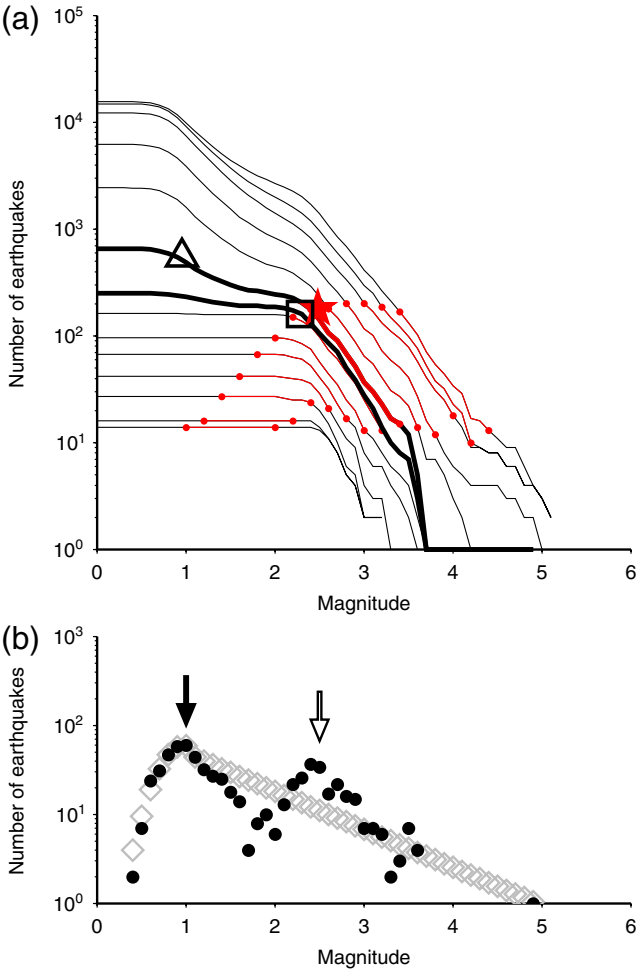

Figure 4. Determination of the M_c using synthetic bimodal FMD and different methods. (a) Cumulative FMDs using concentric circles with different radii at the position 0.7° N, 0.7° E in Figure 3. Using equation (3), highlighted segments located between the dots show the corresponding magnitude ranges. The star indicates the M_c-value predicted by the multiscale method (i.e., the lower limit of the smallest magnitude range over which the GR law is verified). Thick lines with a triangle and a square are the FMDs and the M_c-values obtained by constant radius ($R = 35$ km) and constant sample ($N_c = 250$) methods, respectively. (b) FMD using a radius of 35 km at the same position (upper thick line in part a). The gray diamonds show the best solution of the EMR method. The maximum-likelihood point-estimator method may select a mode (black arrow) that does not correspond to the local M_c (white arrow). The color version of this figure is available only in the electronic edition.

view, the multiscale method presented here may be useful to capture some specific seismic behaviors related to the complexity of volcanic island arcs.

The Seismicity and the Seismic Network of the Lesser Antilles Volcanic Island Arc

The studied region is located at the eastern border of the Caribbean plate between 13° and 18° N latitude and 59° and 63° W longitude (Fig. 5a). This is the central part of the Lesser Antilles volcanic arc where the seismic activity is caused by subduction of Atlantic lithosphere beneath the Caribbean plate with a convergence rate of approximately 2 cm/yr (Demets *et al.*, 2000; Mann *et al.*, 2002). As a result, both volcanic and tectonic earthquakes may be recorded by the local seismic network (Fig. 5a).

Taking advantage of the seismic networks dedicated to monitoring active volcanoes, the recorded volcanic earthquakes are shallow and clustered with low magnitudes (<2.5) if compared with tectonic earthquakes (Fig. 5b). Among these tectonic events, interplate and intraslab earthquakes are expected to be the largest ($M > 8$, according to historical seismicity [Feuillet, Beauducel and Tapponnier, 2011]); for example, the 29 November 2007 M 7.4 intraslab earthquake located north of Martinique at 152 km depth. However, large intraplate earthquakes with a normal faulting mechanism and shallower focal depth may also be observed on a set of faults located in the outer part of the arc (Feuillet *et al.*, 2002). The 21 November 2004 M 6.3 Les Saintes earthquake is an example of this type of seismicity (Bazin *et al.*, 2010; Feuillet, Beauducel, Jacques, *et al.*, 2011).

As with other volcanic island arcs around the world, complex seismic patterns may be observed in the Lesser Antilles using a dense network of seismic stations. In this region, the network developed by the Institut de Physique du Globe de Paris (IPGP) through its volcanological and seismological observatories in Guadeloupe (OVSG) and Martinique (OVSM) is employed. As shown in Figure 5a, the structure of the volcanic island arc does not facilitate the distribution of seismic stations, and the resulting network is highly heterogeneous with a strong meridional alignment. Moreover, a vast majority of earthquakes occur in the outer part of the network (Fig. 5b). Nevertheless, it remains the best network to document seismicity between Antigua and St. Lucia (Bengoubou-Valerius *et al.*, 2008).

The earthquake catalogs of the OVSG and OVSM started officially in 1981. They are homogeneous in content because both networks have been installed and maintained in close collaboration and because both observatories use the same location processes and magnitude calculation (Feuillard, 1985; Clément *et al.*, 2000). Here, we join these two catalogs into a single one using the 15.5° N parallel as a limit for selection. We exclude events with undetermined magnitudes or epicenters and a number of double records. Finally, the combined OVSG–OVSM catalog contains about 25,000 events ranging in magnitude from −0.87 to 7.4. About 80% of these events occur at a depth of less than 40 km. Magnitudes correspond to the classical formula of duration magnitude for $M_D \leq 4.5$ events (Lee *et al.*, 1975), and moment magnitudes from worldwide networks are used for greater events; the consistency of the magnitude scale has already been checked (Clément *et al.*, 2000; Bengoubou-Valerius *et al.*, 2008). Before 1996, magnitudes are given with a resolution of 0.1. For this reason, we only study the combined catalog from 1996 to 2010, for which magnitudes are given with 0.01 resolution. We suppose a constant level of registration during this period because the configuration of the OVSG–OVSM

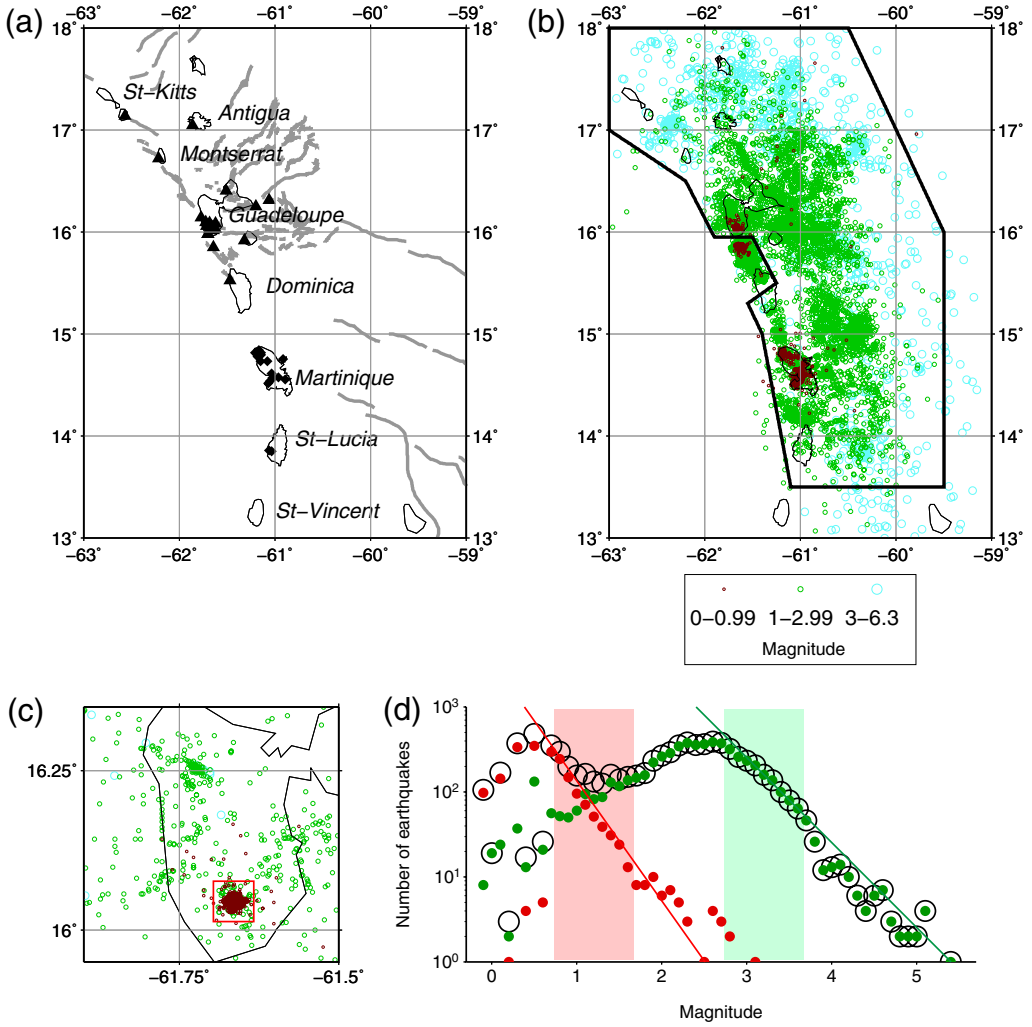

Figure 5. Seismicity of the Lesser Antilles island arc. (a) Location of the seismic stations of the OVSG (triangles) and OVSM (diamonds) networks. Major faults are shown in gray (Feuillet *et al.*, 2002). (b) Distribution of shallow (<40 km) earthquake epicenters in the OVSG–OVSM catalog from 1996 to 2010. Solid black lines limit the region chosen for M_c mapping. (c) Close-up view of the Guadeloupe region in the neighborhood of the La Soufrière volcano (square). (d) Noncumulative FMDs in the entire territory (open circles) and inside (left curve) and outside (right curve) the volcanic area. For each of the two last curves, according to our multiscale procedure, the vertical bands show the lowest magnitude ranges of width $W_M = 1$ for which the FMDs follow the GR law. The color version of this figure is available only in the electronic edition.

network does not change considerably and the number of recorded earthquakes remains stable over time.

The tested region for M_c mapping is shown in Figure 5b. Note that we do not analyze the zone corresponding to the rupture area of the M 6.3 Les Saintes earthquake (Feuillet, Beauducel, Jacques, *et al.*, 2011). In this region, the properties of the catalog are not stationary over time because all the events of the aftershock sequence have not been processed. Hence, the catalog remains incomplete, particularly during the first days after the mainshock. Furthermore, the deployment of a specific network 25 days after the mainshock may authorize more specific and dedicated analysis in the future (Bazin *et al.*, 2010).

Figure 5c shows the distribution of earthquake epicenters in the Guadeloupe region in the neighborhood of the La Soufrière volcano. Given the density of stations in this vicinity, the detection capability is much larger than in the remaining zone. The high detection capability coupled with a high level of seismic activity results in a bimodal FMD for the entire region (Fig. 5d, open circles). This bimodality disappears for FMDs that focus on both the volcanic area and the remaining region. Such an observation clearly illustrates that earthquake patterns depend on both the location and size of seismogenic zones. It also highlights how the multiscale method may be used to estimate M_c and b-values across a wide range of magnitude–space domains (see bandlimited areas in Fig. 5d).

Spatial Variations of the M_c in the Lesser Antilles Volcanic Island Arc

We analyze spatial variations in the M_c in the Lesser Antilles volcanic island arc from 1996 to 2010. We construct

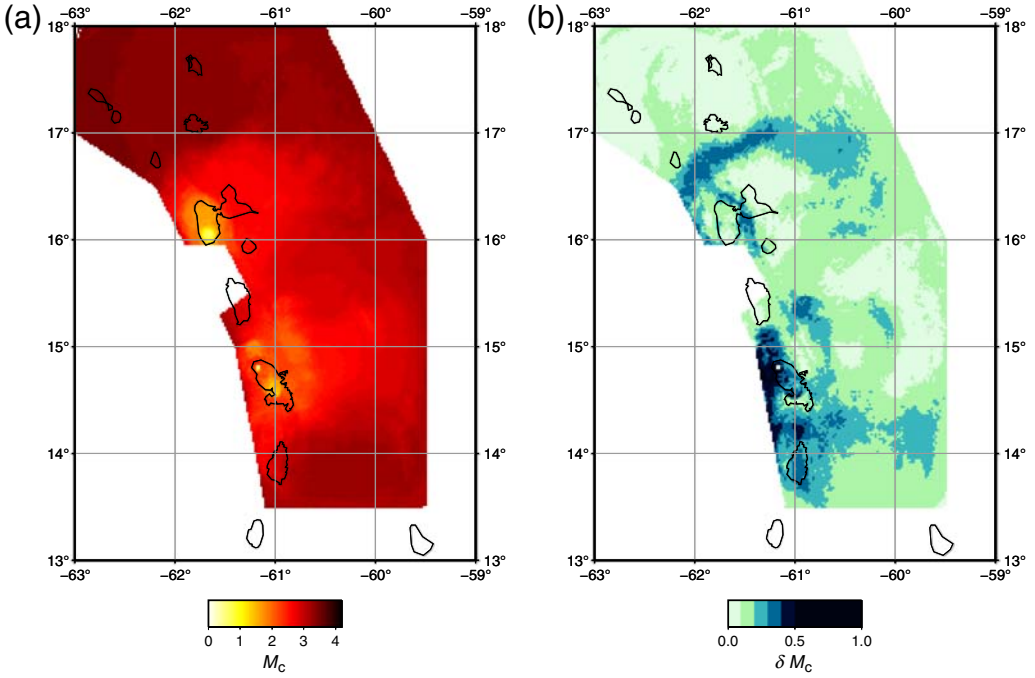

Figure 6. Multiscale M_c-value map of the Lesser Antilles island arc using the OVSG–OVSM catalog: (a) M_c-value map for $R_0 = 50$ km, $p = 0.6$, and $N_c = 50$ events, and (b) δM_c-map using a bootstrap technique (see text). The color version of this figure is available only in the electronic edition.

M_c maps of the OVSG–OVSM earthquake catalog using only $M > 0.5$ events with a focal depth of less than 40 km (Fig. 6a). We use the following set of model parameter values: $W_M = 1$, $\Delta m = 0.1$, $R_0 = 1.3$ km, $p = 0.6$, $N_c = 50$, and grid spacing of 0.02°. In addition, we use the same bootstrap procedure as for tests on synthetic catalogs to generate δM_c maps (Fig. 6b).

Figure 6a shows that the M_c-value varies considerably across the studied territory, increasing with distance from the two main islands of Guadeloupe and Martinique. The best completeness levels of $M_c = 0.7$ and $M_c = 0.5$ correspond to the two large volcanic edifices of La Soufrière (Guadeloupe) and Mount Pelée (Martinique), respectively. Onshore and outside the network dedicated to the volcanoes, $M_c \leq 2.0$, except for the eastern part of Guadeloupe (Grande-Terre). Offshore, $M_c \leq 2.8$ for a distance of < 100 km from the islands. North of the 17° N parallel, $M_c \geq 3.2$. Obviously these results may be directly related to seismicity maps for which we clearly observe that the minimum magnitude of reported events increases with respect to the distance to Guadeloupe and Martinique (Fig. 5b). Nevertheless, we now have a precise quantitative tool that allows a more detailed study of the recording capacity of the local seismic station network.

Let us consider three points A, B, and C located on the La Soufrière volcano and onshore and offshore of Guadeloupe island, respectively (Fig. 7a,b). The distance between these points is approximately 25 km, but the local levels of completeness of the catalog differ significantly from $M_c = 0.7$ in A to $M_c = 2.6$ in C. Hence, each point is associated to different space–magnitude scales: $R_A = 4.5$ km and $\mathcal{M}_A = [0.7, 1.7]$ (Fig. 7b and 7c), $R_B = 13$ km and $\mathcal{M}_B = [1.6, 2.6]$ (Fig. 7b and 7d), and $R_C = 51$ km and $\mathcal{M}_C = [2.6, 3.6]$ (Fig. 7b and 7e). Each of these space–magnitude scales is locally the best to yield a statistically significant estimation of the M_c-value. In addition, by using all the parameters documented in the catalog and the corresponding b-values, the multiscale method may contribute to a better characterization of the local seismic patterns. For example, looking at the depth of the selected events and their corresponding b-values, we have here $h_A = 0.3 \pm 1.5$ km and $b_A = 1.33 \pm 0.03$, $h_B = 8.5 \pm 7.2$ km and $b_B = 0.86 \pm 0.08$, and $h_C = 16.4 \pm 10.5$ km and $b_C = 1.43 \pm 0.06$. The multiscale methods may therefore be used to analyze seismicity and recognize characteristic earthquake patterns associated with different types of seismogenic mechanisms, especially in volcanic island arcs.

Figure 6b shows that, in a vast majority of cases, δM_c-values are less than 0.2 across the entire territory (median value is 0.13). These low values may be explained by the number of events selected at each point. The actual sample size is more than 100 in at least 80% of the territory (median value is 175). The maximum uncertainty $\delta M_c > 0.5$ is observed northward of Martinique and can be explained by the small sample size (< 100) in this region of low seismic activity. As shown by the synthetic catalogs (see Fig. 3), narrow bands of larger δM_c-values may be related to sharp changes of detection capability. Such a relation between changes in M_c-value and the amplitude of the δM_c-value is also illustrated in Figure 8. It confirms that abrupt changes

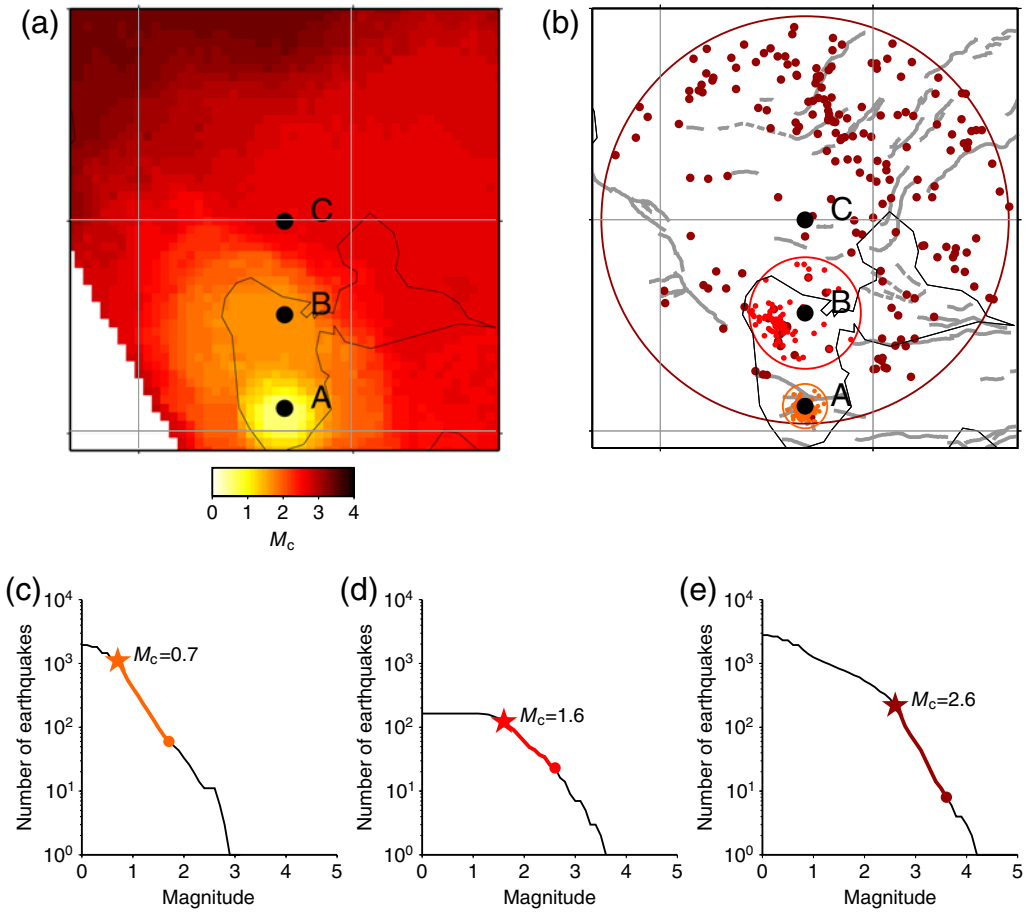

Figure 7. Local determination of the M_c-value in three different volcanotectonic settings in the neighborhood of the La Soufrière volcano in Guadeloupe. (a) M_c-value map. Aligned along the 61.66° W meridian, points A (16.04° N, $M_c = 0.7$), B (16.28° N, $M_c = 1.6$), and C (16.50° N, $M_c = 2.6$) correspond to a volcanic, an onshore, and an offshore zone of seismic activity. (b) Earthquakes and circles used to determine the M_c-value at points A, B, and C. The corresponding radii and magnitude ranges are $R_A = 4.5$ km and $\mathcal{M}_A = [0.7, 1.7]$, $R_B = 13$ km and $\mathcal{M}_B = [1.6, 2.6]$, and $R_C = 51$ km and $\mathcal{M}_C = [2.6, 3.6]$. (c–e) Cumulative FMDs and the corresponding magnitude ranges located between dot and star and used to determine the M_c-value at points A (c), B (d), and C (e). The color version of this figure is available only in the electronic edition.

of the M_c-value (Fig. 8a) are associated with maxima of the δM_c-value (Fig. 8b).

Most importantly for our present purpose, Figure 8 also shows that the multiscale method is able to identify discontinuities in detection capability. In fact, the correlation between our M_c-value estimates (Fig. 8a) and the mean magnitude of all recorded earthquakes in this zone (Fig. 8c) seems to indicate that the method is precise enough to characterize potential artifacts of seismic catalogs.

Comparison with Other Methods

Sharp changes of seismic activity and/or discontinuous levels of registration may produce FMD that do not satisfy the GR law (e.g., bimodal FMD). Then, the size of the area for data selection may have an impact on M_c-value estimates. For comparison with our multiscale technique, we use classical catalog-based methods to map the M_c-value of the Lesser Antilles island arc. For the constant radius (Fig. 9a) and sample size methods (Fig. 9b), we obtain results that are similar to those obtained using synthetic data. Indeed, the M_c-values of more seismically active zones expand into zones of lower activity, and the surface areas with high level of completeness are systematically larger than those calculated by the multiscale approach.

We next try to apply the Bayesian method proposed by Mignan *et al.* (2011). This method includes a step in which catalog and network information are combined to determine the length scale for data selection. This step therefore provides an effective way of deriving the mapping resolution from data. Unfortunately, it cannot be automatically applied in zones where the distribution of seismic stations is too sparse and clustered. Following the advice of A. Mignan (personal comm., 2012), we assume that the specific length scales for data selection derived from the Taiwan case are also valid in the Lesser Antilles. Using these specific length scales to select an earthquake in the OVSG–OVSM catalog, we also apply the same maximum-curvature method to

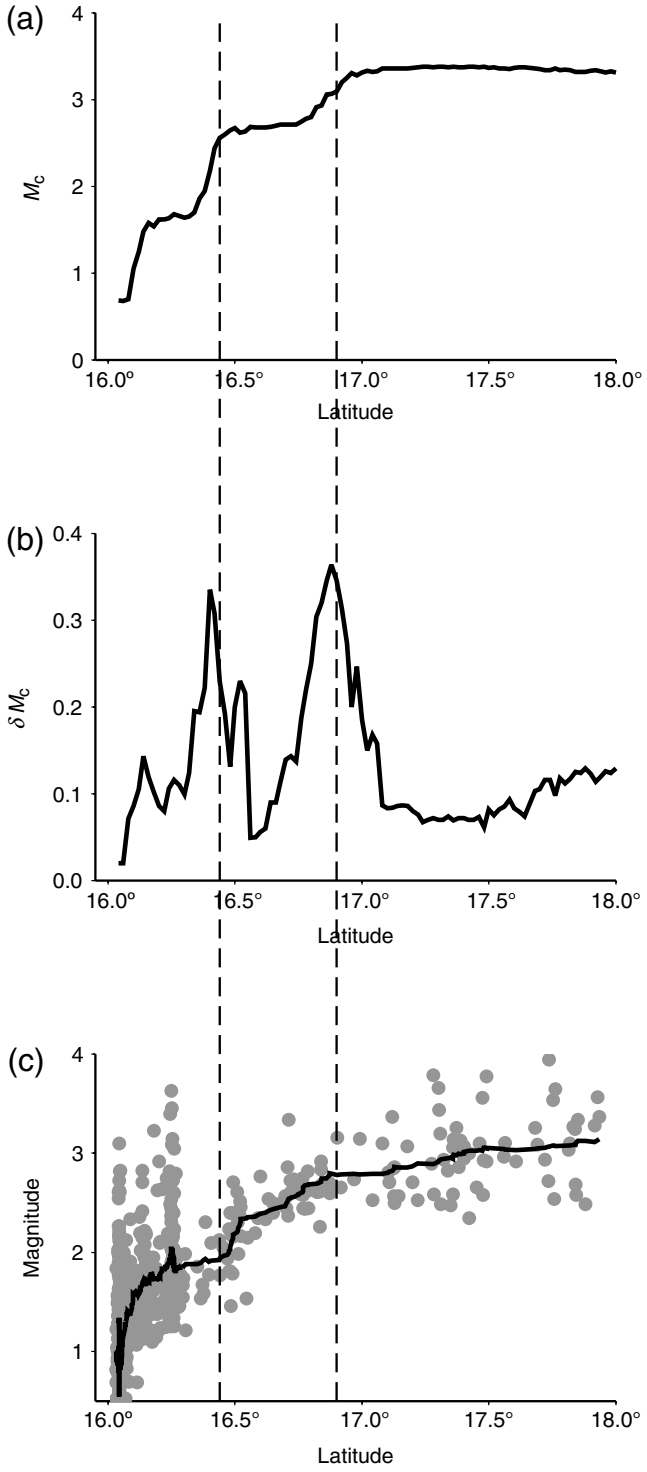

Figure 8. Properties of the combined OVSG–OVSM catalog along a meridian north of the La Soufrière volcano: (a) M_c-value and (b) δM_c-value along the 61.66° W meridian, and (c) magnitudes of earthquakes located between the 61.50° W and the 61.80° W meridians. The solid black line is the mean magnitude of the recorded earthquakes (gray dots) using a sliding window with constant number of event ($N = 50$). Dashed lines are associated with a sharp transition of the detection capability.

locally determine the M_c-value (Mignan *et al.*, 2011). A direct comparison between the M_c-value maps obtained by the multiscale (Fig. 6a) and the Bayesian methods (Fig. 9c) shows that both approaches produce comparable results and achieve the same spatial resolution.

To explain these similarities, we compare the local optimized length scale for data selection obtained in Taiwan ($\Delta d/2$ using equations 1 and 2 of Mignan *et al.*, 2011) to those obtained by our multiscale approach using equation (3). Not surprisingly, Figure 10 shows that both length scales exhibit the same dependency on the M_c-value. However, for the same M_c-value, the length scale obtained from the distribution of seismic stations in Taiwan is three times smaller than in the multiscale approach. This difference depends only on the particular choice of the R_0-value. A smaller value may be chosen to the detriment of the statistical significance in the estimation of the FMDs within specific magnitude ranges.

Concluding Remarks

We propose a new multiscale method for the estimation of spatially varying M_c. In this method local seismicity is analyzed within a discrete set of magnitude–space domains. The underlying hypothesis is therefore that there is not a unique relationship for the description of seismicity within all these domains. In practice, the entire formalism of the multiscale method is based on empirical relations (equations 1 and 2) that locally determine the characteristic length scale for event selection with respect to the magnitude range through which these specific earthquakes have to be examined.

Evaluation tests on synthetic and instrumental catalogs demonstrate that the multiscale method allows correct delineation of zones with different levels of completeness. The high resolution capacity of the method arises from the automatic choice of the proper magnitude–space domain of the recorded seismicity at any point in space. As a result, the multiscale method is also efficient for identifying abrupt changes in the detection threshold.

The multiscale method is complementary to traditional catalog-based approaches because it is based on a self-adjusting mechanism that replaces the traditional parametrization of local earthquake selection (e.g., radius, circle, and sample size). Thus, it explores all length scales, considering for each a magnitude range that guarantees the statistical significance of the results. As for other GR-based methods that compute the M_c of the samples, our new method also includes some sort of averaging over space. If this effect is significantly reduced by the multiscale sampling, it still remains to a lesser degree. In this case, the method may not always guarantee an optimal choice of the region size corresponding to a driving earthquake mechanism.

Furthermore, the multiscale method may have advantages for which network analysis methods are difficult to implement. This is, for example, the case for the Bayesian

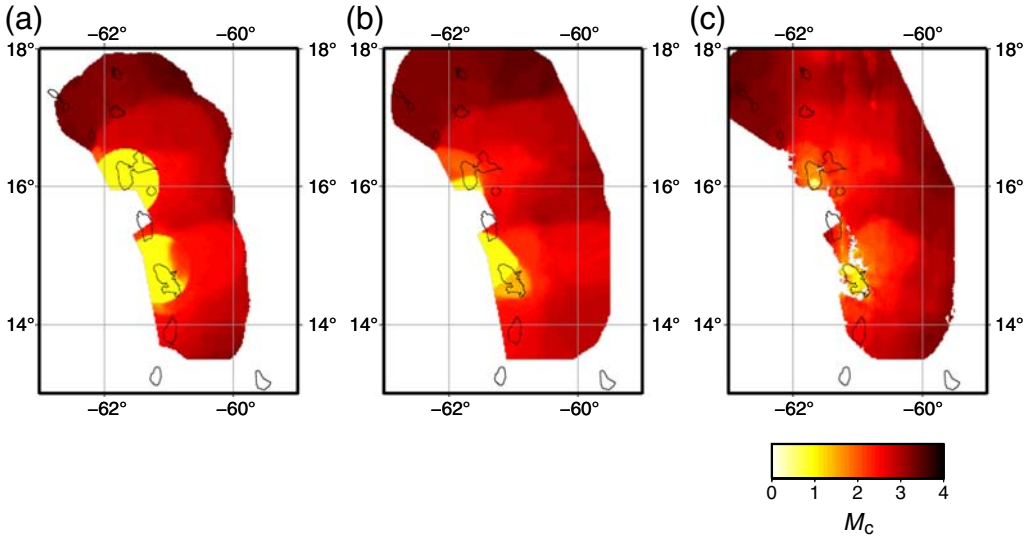

Figure 9. Alternative methods for mapping the M_c-value of the Lesser Antilles island arc using the OVSG–OVSM catalog: (a) the constant radius method with $R = 55$ km, (b) the constant sample size method with $N_c = 250$, and (c) the Bayesian method of Mignan *et al.* (2011). The local length scales for data selection is determined from the results obtained in Taiwan; the M_c-value is determined by the maximum-curvature method. The color version of this figure is available only in the electronic edition.

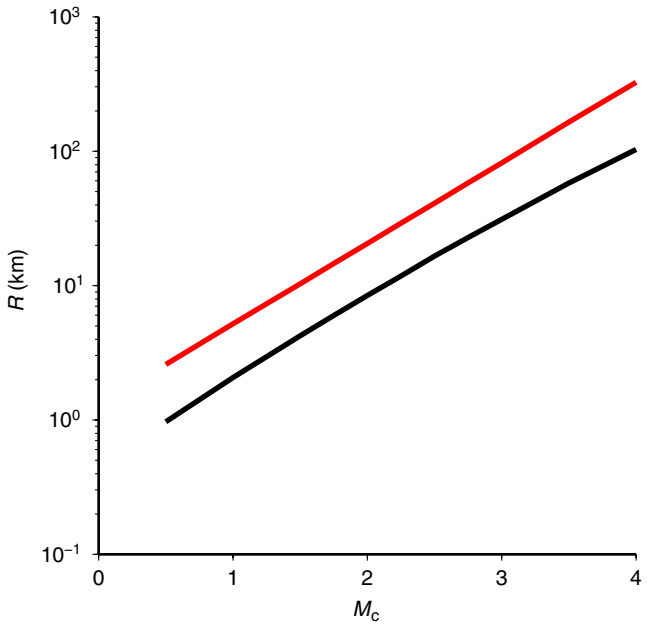

Figure 10. Relationship between the characteristic length scale for data selection and the M_c-value for the multiscale (upper line) and the Bayesian methods (lower line) of Mignan *et al.* (2011). The same order of magnitude and the similar dependency indicate that the multiscale approach is able to identify a relevant length scale for data selection. The color version of this figure is available only in the electronic edition.

approach of Mignan *et al.* (2011) in the Lesser Antilles volcanic island arc because of the configuration of the seismic network. In this specific region, the best-fit relationship between M_c and the distance d from the nth station is too flat for large distances (see Fig. 8c), and the radius of the area for event selection becomes rapidly larger than the size of the studied region. Hence, the multiscale method is an alternative in zones where recorded seismicity and network configuration do not allow construction of a satisfactory regional relation between M_c and the proximity to the network.

As for all catalog-based approaches, the multiscale method cannot fully overcome difficulties in M_c mapping in aseismic or low seismic areas. However, we address this issue for the first time, and local estimates obtained by the multiscale method are statistically significant upper limits of the real M_c-values. On the other hand, instrumental catalogs also span a certain period, often many years. In this case, the obtained M_c-value estimates represent some sort of averaging over time. This effect may be critical as short bursts of low-magnitude seismicity can easily become the dominant part of the FMD. In addition, seismic stations often operate only intermittently, causing strong drops in completeness, which are invisible to catalog-based methods (Nanjo, Schorlemmer, *et al.*, 2010; Schorlemmer *et al.*, 2010). At this stage the multiscale method does not address this problem at all. Nevertheless, its temporal counterpart may be elaborated on the basis of a relationship between a period for data collection and a magnitude range (see equation 3). This is a clear direction of research in the field of historical seismicity but also enables us to discuss time-varying completeness levels in a specific area.

At this stage, we only concentrate on the M_c using the smallest magnitude range in which the GR law is verified. Nevertheless, the method can also be used to isolate specific seismic patterns by analyzing all magnitude–space domains across the entire territory. The results obtained in the Lesser Antilles volcanic island arc illustrate the feasibility of this

approach that will be developed in different zones of seismic activity.

Data and Resources

The earthquake catalogs used in this study are provided by the Institut de Physique du Globe de Paris (IPGP) through its volcanological and seismological observatories in Guadeloupe (OVSG) and Martinique (OVSM) (Feuillard, 1985; Clément *et al.*, 2000).

Acknowledgments

The paper has been improved by constructive comments from two anonymous reviewers. Authors thank the staff at the Guadeloupe and Martinique observatories and especially their successive directors, M. Feuillard, J.-C. Komorowski, J.-B. de Chabalier, J.-P. Viodé, and S. Bazin, for their contribution in producing the catalogs. This work has been partially supported by the French Ministry of Research (ANR-09-RISK-02-001/CASAVA) and the Russian Foundation for Basic Research (11-05-00530).

References

Aki, K. (1965). Maximum likelihood estimate of b in the formula $\log N = a - bM$ and its confidence level, *Bull. Earthq. Res. Inst.* **43,** 237–239.

Amorèse, D. (2007). Applying a change-point detection method on frequency-magnitude distributions, *Bull. Seismol. Soc. Am.* **97,** doi: 10.1785/0120060181.

Bazin, S., N. Feuillet, C. Duclos, W. Crawford, A. Nercessian, M. Bengoubou-Valérius, F. Beauducel, and S. Singh (2010). The 2004–2005 Les Saintes (French West Indies) seismic aftershock sequence observed with ocean bottom seismometers, *Tectonophysics* **489,** 91–103, doi: 10.1016/j.tecto.2010.04.005.

Bender, B. (1983). Maximum likelihood estimation of b-values for magnitude grouped data, *Bull. Seismol. Soc. Am.* **73,** 831–851.

Bengoubou-Valerius, M., S. Bazin, D. Bertil, F. Beauducel, and A. Bosson (2008). CDSA: A New Seismological Data Center for the French Lesser Antilles, *Seismol. Res. Lett.* **79,** 90–102.

Ben-Zion, Y. (2008). Collective behavior of earthquakes and faults: Continuum-discrete transitions, progressive evolutionary changes and different dynamic regimes, *Rev. Geophys.* **46,** RG4006, doi: 10.1029/2008RG000260.

Cao, A. M., and S. S. Gao (2002). Temporal variation of seismic b-values beneath northeastern Japan island arc, *Geophys. Res. Lett.* **29,** doi: 10.1029/2001GL013775.

Clément, C., P. Bernard, J. Viodé, C. Anténor-Habazac, J. Lépine, and F. Beauducel (2000). Compilation et validation du catalogue de sismicité des observatoires IPGP des Antilles, *Tech. Rept.*, Ministère de l'Aménagement du Territoire et de l'Environnement, Institut de Physique du Globe de Paris (in French).

Demets, C., P. Jansma, G. Mattioli, T. Dixon, F. Farina, R. Bilham, E. Calais, and P. Mann (2000). GPS geodetic constraints on Caribbean–North America plate motion, *Geophys. Res. Lett.* **27,** 437–440.

Farrell, J., S. Husen, and R. B. Smith (2009). Earthquake swarm and b-value characterization of the Yellowstone volcano-tectonic system, *J. Volcanol. Geoth. Res.* **188,** 260–276, doi: 10.1016/j.jvolgeores.2009.08.008.

Feuillard, M. (1985). Macrosismicité de la Guadeloupe et de la Martinique, *Ph.D. Thesis*, Institut de Physique du Globe de Paris (in French).

Feuillet, N., F. Beauducel, E. Jacques, P. Tapponnier, P. Delouis, S. Bazin, M. Vallée, and G. King (2011). The $M_w = 6.3$, November 21, 2004, Les Saintes earthquake (Guadeloupe): Tectonic setting, slip model and static stress changes, *J. Geophys. Res.* **116,** no. B10, 301, doi: 10.1029/2011JB008310.

Feuillet, N., F. Beauducel, and P. Tapponnier (2011). Tectonic context of moderate to large historical earthquakes in the Lesser Antilles and mechanical coupling with volcanoes, *J. Geophys. Res.* **116,** B10308, doi: 10.1029/2011JB008443.

Feuillet, N., I. Manighetti, P. Tapponnier, and E. Jacques (2002). Arc parallel extension and localization of volcanic complexes in Guadeloupe, Lesser Antilles, *J. Geophys. Res.* **107,** no. B12, 2331, doi: 10.1029/2001JB000308.

Gomberg, J. (1991). Seismicity and detection/location threshold in the southern Great Basin seismic network, *J. Geophys. Res.* **96,** 401–414.

Gutenberg, B., and C. F. Richter (1944). Frequency of earthquakes in California, *Bull. Seismol. Soc. Am.* **34,** 185–188.

Ishimoto, M., and K. Iida (1939). Observations of earthquakes registered with the microseismograph constructed recently, *Bull. Earthq. Res. Inst.* **17,** 443–478.

Kanamori, H., and D. L. Anderson (1975). Theoretical basis of some empirical relations in seismology, *Bull. Seismol. Soc. Am.* **65,** no. 5, 1073–1095.

King, G. (1983). The accommodation of large strain in the upper lithosphere of the Earth and other solids by self-similar fault systems, *Pure Appl. Geophys.* **121,** 761–815.

Kvaerna, T., F. Ringdal, J. Schweitzer, and L. Taylor (2002a). Optimized seismic threshold monitoring—part 1: Regional processing, *Pure Appl. Geophys.* **159,** 969–987.

Kvaerna, T., F. Ringdal, J. Schweitzer, and L. Taylor (2002b). Optimized seismic threshold monitoring—part 2: Regional processing, *Pure Appl. Geophys.* **159,** 989–1004.

Lee, W., and J. Lahr (1975). HYPO71 (Revised): A computer program for determining hypocenter, magnitude, and first motion pattern of local earthquakes, *U.S. Geol. Surv. Open-File Rept. 75-311*.

Mann, P., E. Calais, J. Ruegg, C. Demets, P. Jansma, and G. Mattioli (2002). Oblique collision in the northeastern Caribbean from GPS measurements and geological observations, *Tectonics* **21,** 1057.

Mignan, A., and J. Woessner (2012). Estimating the magnitude of completeness for earthquake catalogs, *Community Online Resource for Statistical Seismicity Analysis*, doi: 10.5078/corssa-00180805.

Mignan, A., M. Werner, S. Wiemer, C.-C. Chen, and Y.-M. Wu (2011). Bayesian estimation of the spatially varying completeness magnitude of earthquake catalogs, *Bull. Seismol. Soc. Am.* **101,** 1371–1385.

Molchan, G., T. Kronrod, and G. Panza (1997). Multi-scale seismicity model for seismic risk, *Bull. Seismol. Soc. Am.* **87,** no. 5, 1220–1229.

Nanjo, K., T. Ishibe, H. Tsuruoka, D. Schorlemmer, Y. Ishigaki, and N. Hirata (2010). Analysis of the completeness magnitude and seismic network coverage of Japan, *Bull. Seismol. Soc. Am.* **100,** 3261–3268.

Nanjo, K., D. Schorlemmer, J. Woessner, S. Wiemer, and D. Giardini (2010). Earthquake detection capability of the Swiss Seismic Network, *Geophys. J. Int.* **181,** 1713–1724.

Narteau, C., S. Byrdina, P. Shebalin, and D. Schorlemmer (2009). Common dependence on stress for the two fundamental laws of statistical seismology, *Nature* **462,** 642–645, doi: 10.1038/nature08553.

Narteau, C., P. Shebalin, and M. Holschneider (2002). Temporal limits of the power law aftershock decay rate, *J. Geophys. Res.* **107,** doi: 10.1029/2002JB001868.

Narteau, C., P. Shebalin, G. Zöller, S. Hainzl, and M. Holschneider (2003). Emergence of a band-limited power law in the aftershock decay rate of a slider-block model of seismicity, *Geophys. Res. Lett.* **30,** doi: 10.1029/2003GL017110.

Ogata, Y., and K. Katsura (1993). Analysis of temporal and spatial heterogeneity of magnitude frequency distribution inferred from earthquake catalogs, *Geophys. J. Int.* **113,** 727–738.

Rydelek, P. A., and I. S. Sacks (1989). Testing the completeness of earthquake catalogs and the hypothesis of self-similarity, *Nature* **337,** 251–253.

Rydelek, P. A., and I. S. Sacks (2003). Comment on "Minimum magnitude of completeness in earthquake catalogs: Examples from Alaska, the

western United States, and Japan" by Stefan Wiemer and Max Wyss, *Bull. Seismol. Soc. Am.* **93,** 1862–1867.

Sagar, S., and M. Leonard (2007). Mapping the magnitude of completeness of the Australian earthquake catalog, in *Proc. Aust. Earthquake Eng. Soc. Conf.*, Wollongong NSW, Australia, 23–25 November 2007.

Schorlemmer, D., and J. Woessner (2008). Probability of detecting an earthquake, *Bull. Seismol. Soc. Am.* **98,** no. 5, 2103–2117, doi: 10.1785/0120070105.

Schorlemmer, D., A. Christophersen, A. Rovida, F. Mele, M. Stucchi, and W. Marzocchi (2010). Setting up an earthquake forecast experiment in Italy, *Ann. Geophys.* **53,** no. 3, doi: 10.4401/ag-4844.

Schorlemmer, D., S. Wiemer, and M. Wyss (2005). Variations in earthquake-size distribution across different stress regimes, *Nature* **437,** no. 7058, 539–542.

Schwartz, D., and K. Coppersmith (1984). Fault behavior and characteristic earthquake: Examples from the Wasatch and San Andreas fault zones, *J. Geophys. Res.* **89,** no. B7, 5681–5698.

Segall, P. (2010). *Earthquake and Volcano Deformation*, Princetown University Press.

Shi, Y., and B. Bolt (1982). The standard error of the magnitude–frequency *b*-value, *Bull. Seismol. Soc. Am.* **72,** 1677–1687.

Wells, D., and K. Coppersmith (1994). New empirical relationships among magnitude, rupture length, rupture width, rupture area, and surface displacement, *Bull. Seismol. Soc. Am.* **84,** 974–1002.

Wesnousky, S. (1994). The Gutenberg–Richter or characteristic earthquake distribution, which is it? *Bull. Seismol. Soc. Am.* **84,** no. 6, 1940–1959.

Wiemer, S., and M. Wyss (2000). Minimum magnitude of completeness in earthquake catalogs: Examples from Alaska, the western United States, and Japan, *Bull. Seismol. Soc. Am.* **90,** 859–869.

Woessner, J., and S. Wiemer (2005). Assessing the quality of earthquake catalogues: Estimating the magnitude of completeness and its uncertainty, *Bull. Seismol. Soc. Am.* **95,** 684–698.

Institute of Earthquake Prediction Theory and Mathematical Geophysics
618 Russian Academy of Sciences
84/32 Profsouznaya
Moscow 117997, Russia
vorobiev@mitp.ru
(I.V., P.S.)

Institut de Physique du Globe de Paris
Sorbonne Paris Cité
Univ. Paris Diderot
UMR 7154 CNRS
1 rue Jussieu
75238 Paris, Cedex 05, France
(C.N., F.B., A.N.)

Observatoire Volcanologique et Sismologique de Martinique
Institut de Physique du Globe de Paris
Morne des Cadets
97250 Fonds Saint Denis
La Martinique, French West Indies
(V.C.)

Observatoire Volcanologique et Sismologique de Guadeloupe
Institut de Physique du Globe de Paris
Le Houëlmont
97113 Gourbeyre
La Guadeloupe, French West Indies
(M.-P.B.)

Manuscript received 6 April 2012